Electronic Supplementary Material (ESI) for Inorganic Chemistry Frontiers.

Supporting Information

Ultrafast and Durable Li/Na storage by an Iron Selenide Anode Using an Elastic Hierarchical Structure

Peng Jing,[a] *Qiong Wang,*[a] *Chunxiang Xian,*[a] *Liyu Du,*[a] *Yin Zhang,*[a] *Boya Wang,*[a] *Hao Wu,*[a, b] *Kaipeng Wu,*[a, b] *Qian Wang*[*],[a, b] *Yun Zhang*[*],[a, b]

[a] Department of Advanced Energy Materials, College of Materials Science and Engineering, Sichuan University, Chengdu 610064, PR China

[b] Engineering Research Center of Alternative Energy Materials & Devices, Ministry of Education, Sichuan University, Chengdu 610064, PR China

[*] **Corresponding authors**: Yun Zhang, Qian Wang

Emails: y_zhang@scu.edu.cn; wangqian1215@scu.edu.cn

Contents

Experimental Section

Materials

Chemical agents including Fe_2O_3, sucrose, and Se powder were bought from Shanghai Aladdin Biochemical Technology Co. Ltd (China). Graphene oxide powder were bought from Suzhou Tanfeng Graphene Technology Co. Ltd (China). All chemicals were directly used without any further treatment.

Preparation of Fe_3O_4/C microspheres: Fe_3O_4/C microspheres were synthesized through a facile spray drying method, as reported in our previous work. [S1] Briefly, 5 g commercial Fe_2O_3 nanoparticles and 3 g sucrose were dispersed and dissolved into 50 mL purified water under vigorous ultrasonication to form a homogeneous dark-red slurry. Then, this slurry was sprayed to generate numerous small droplets and dried concurrently under a hot air flow with 200 ℃. The dried powder was collected by a cyclone separator, which was denoted as Fe_2O_3/sucrose. Finally, the Fe_2O_3/Sucrose hybrids were calcined at 550 ℃ for 3 h under Ar atmosphere to obtained the target Fe_3O_4/C microspheres.

***Preparation of GO@Fe_3O_4/C hybrids*:** Typically, 100 mg as-prepared Fe_3O_4/C composite was dispersed into 100 mL of 5 wt% PDDA aqueous solution to form a uniform suspension under ultrasonic treatment, and stirred for 1 h. To separated PDDA-modified Fe_3O_4/C particles and redundant PDDA, the mixture was centrifugated using deionized water for several times. Subsequently, the PDDA-modified Fe_3O_4/C precipitate was re-dispersed to 50 mL deionized water, and then this mixture was slowly dropped into 20 mL graphene oxide (GO) aqueous suspension (1 mg mL^{-1}) under magnetic stirring. In this process, the negatively charged GO sheets were adhered tightly on the surface of the positively charged PDDA-modified Fe_3O_4/C particles under electrostatic attraction. Finally, the GO@Fe_3O_4/C hybrids were obtained through centrifugation and freeze-drying.

***Preparation of GF@FeSe/C composites*:** In this process, the as-prepared GO@Fe_3O_4/C hybrids and selenium powder were replaced at two separate positions in one porcelain crucible with a weight ratio of 1:2 and then the crucible was moved into a furnace tube with an Ar/H_2

(5%) filled atmosphere. After heated at 400 °C for 6 h and at 600 °C for another 2 h with a rate of 2 °C min^{-1}, the GO@Fe_3O_4/C were completely converted to the target GF@FeSe/C products.

For comparison, FeSe bulks and FeSe/C were also synthesized using pure Fe_2O_3 and Fe_3O_4/C microspheres as the precursor in the same selenylation way as the GF@ FeSe/C composite, respectively.

Characterization

Field emission scanning electron microscopy (FE-SEM, Hitachi, S-4800, Japan) and field emission transmission electron microscopy (TEM, FEI, Titan themis 200, USA) were employed to observe the morphology and microstructure of the materials. Powder X-ray diffraction (XRD, Philips X'pert TROMPD, Cu Kα1 radiation, λ=1.54178 Å) was applied to identify the crystalline phases. The chemical composition and their valences were further investigated by X-ray photoelectron spectrometer (XPS, Escalab 250, Thermo Fischer Scientific, USA). Raman spectra were recorded on a Raman spectrophotometer (Horiba Jobin Yvon, HR800, France) with 532.17 nm laser radiation. The elemental contents were determined through elemental analysis technique.

Electrochemical Measurements

The electrochemical properties of all the samples were tested with a half-cell LIBs and SIBs configuration. To prepared the working electrode, the 70 wt.% active materials, 20 wt.% acetylene black, and 10 wt.% sodium polyacrylate were pre-mixed in deionized water to from a homogenous slurry, and then the slurry was cast onto copper foil and dried at 80 °C in a vacuum for 4 h. After dried treatment, the sheet was punched into disc (Φ=12 mm) as the final working electrode, where the mass loading of active materials (e.g. GF/FeS_2@C) is about 1.0-1.5 mg cm^{-1}. For LIBs, the half cells (type CR2032) were assembled by using lithium metal foil and Celgard 2400 as counter electrode and separator, respectively. The electrolyte was consisted of 1 M $LiPF_6$ in ethylene carbonate/diethyl carbonate (1:1 by volume) with the

addition of volumetric 5 % fluoroethylene carbonate. For half cells of SIBs (type CR2016), sodium metal foil and Whatman glass fiber were used as counter electrode and separator, respectively. And 1.0 M $NaCF_3SO_3$ in diglyme (DGM) was used as the electrolyte.

Electrochemical performances including rate ability, cycling capability and discharge-charge curves were tested using an automatic NEWARE battery cycler (Neware, China). For LIBs and SIBs, the testing voltage window was 0.01-3 V and 0.5-3 V, respectively. Cyclic voltammetry (CV) and Electrochemical impedance spectra (EIS) analysis were performed by a PARSTAT multichannel electrochemical workstation (Princeton Applied Research, PMC1000DC, USA). EIS measurements were conducted at a frequency range of 0.01–100 kHz with the voltage perturbation at 5 mV. The capacity of the electrode was calculated based on the total weight of the samples.

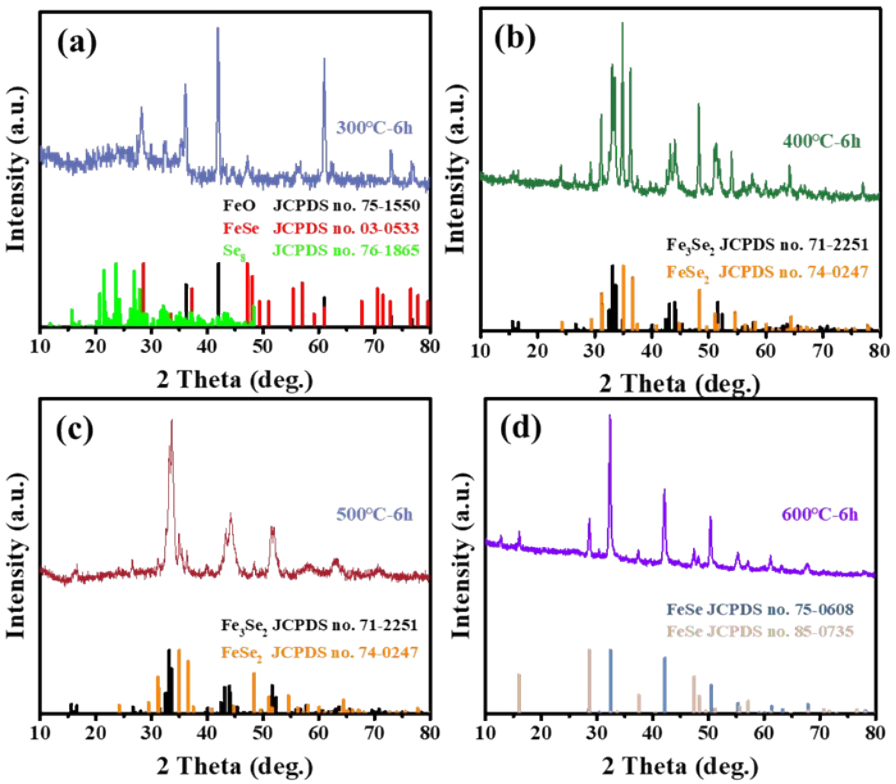

Figure S1. XRD pattern of the iron selenide sample synthesized at (a) 300 ℃, (b) 400 ℃, (c) 500 ℃, and (d) 600 ℃ for 6 h.

As shown in **Figure S1**, when annealing at 300 ℃ for 6h, as seen in **Figure S1a**, the product shows the peaks of both FeO, FeSe, and Se_8, indicating an uncompleted selenylation level of Fe_3O_4@C. The gaseous Se was adsorbed into the pore of Fe_3O_4@C and coagulated to form Se_8 molecule under a low temperature of 300 ℃, which was why the sample showed the diffraction peaks of Se_8. Increasing the temperature to 400 or 500 ℃, all Fe_3O_4@C was translated into $FeSe_2$ and Fe_3Se_2 without the remnant of Se (**Figure S1b and c**). At 600 ℃, the peaks of the as-obtained iron selenide is matched well with FeSe crystal (**Figure RS1d**), demonstrating the complete chemical reaction and high purity of

FeSe. This result suggests that high annealing temperature is helpful to synthesize high purity FeSe. It should be pointed out that the FeSe product synthesized directly at 600 ℃ exhibits both hexagonal and tetragonal structure. However, the FeSe sample obtained in our work is only matched with the tetragonal layered FeSe, suggesting that the two-steps selenylation program enhances the crystallization and helps to improve the phase purity of the final product.

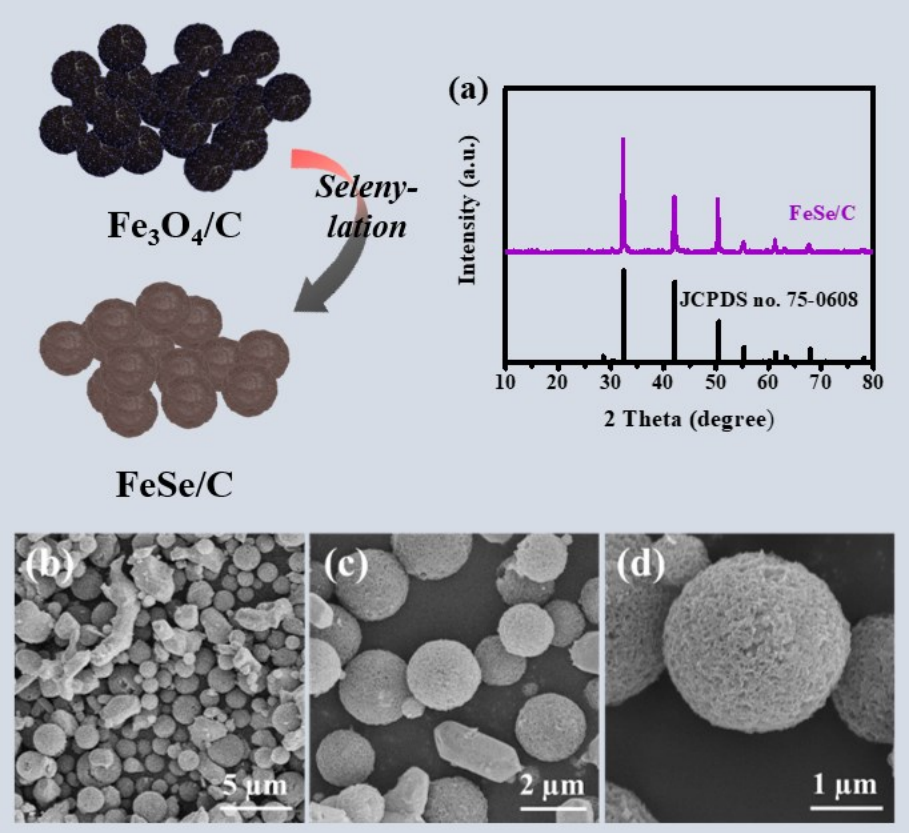

Figure S2. Schematic illustration of the synthesis process for the FeSe/C microspheres. (a) XRD pattern, and (b-d) SEM images of the FeSe/C microspheres.

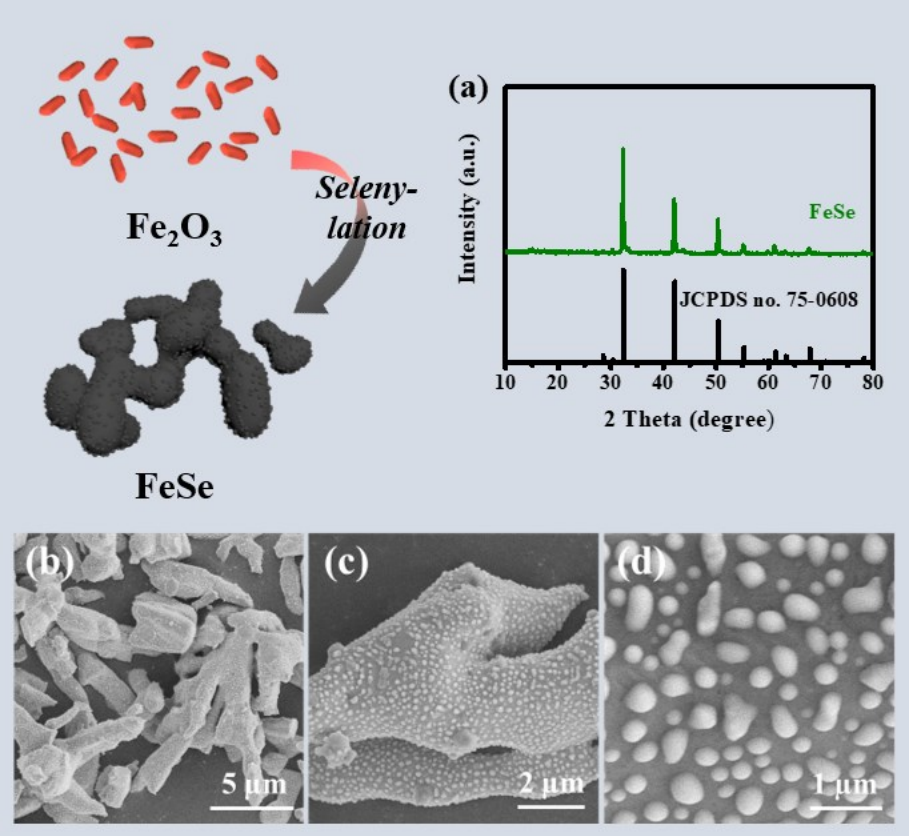

Figure S3. Schematic illustration of the synthesis process for the FeSe bulks. (a) XRD pattern, and (b-d) SEM images of the FeSe bulks.

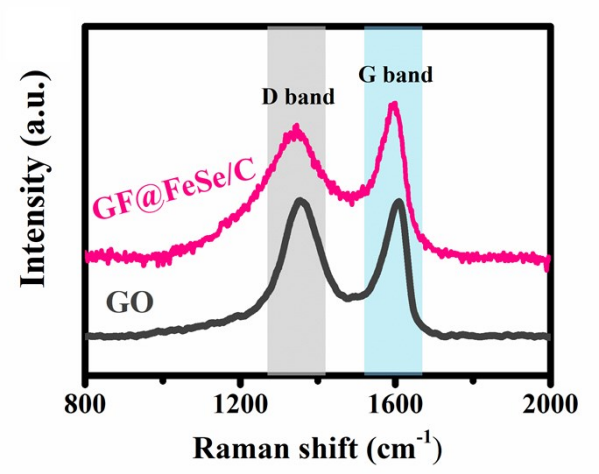

Figure S4. Raman spectra of the GF@FeSe/C and GO.

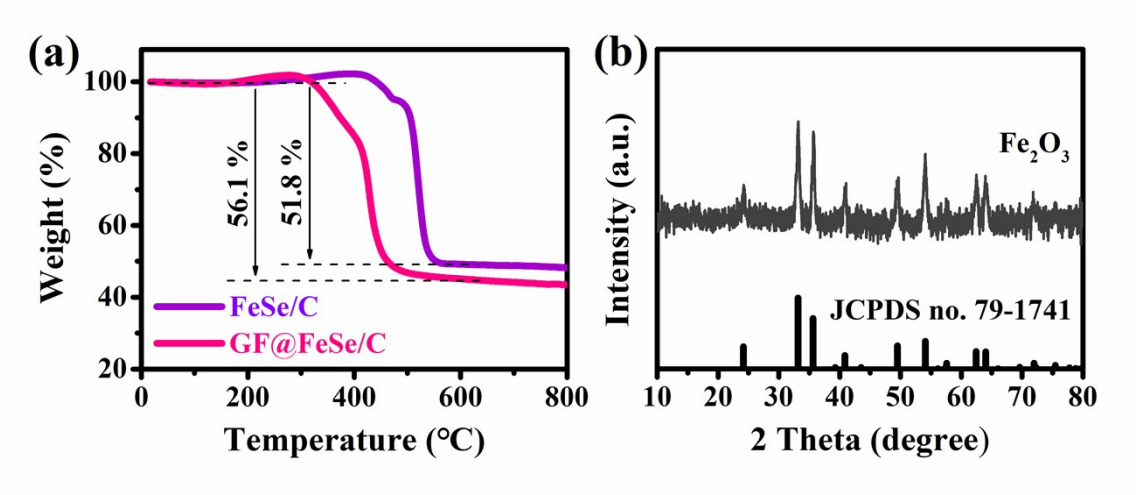

Figure S5. (a) TG curves of the GF@FeSe/C and FeSe/C composites. (b) XRD pattern of GF@FeSe/C after burned at 800 ℃ in Air.

As shown in **Figure S4a**, the main weight loss of both FeSe/C and GF@FeSe/C samples occurs in the temperature range of 300 to 700 °C, which is originated from two parts including the combustion of carbonaceous components and the oxidation reaction from FeSe to Fe_2O_3, as verified by the postmortem XRD result (**Figure S4b**). Assuming the carbon content in the samples is x, the x value can be calculated using the following formula:

$$FeSe\ (s) \rightarrow 1/2\ Fe_2O_3\ (s) + 1/2\ SeO_2\ (g)$$

Mr: 134.85 159.7

m: (1-x) 0.592 (1-x)

For FeSe/C sample: $0.592\ (1 - x) = 1\text{-}51.8\ \%$

For GF@FeSe/C sample: $0.592\ (1 - x) = 1\text{-}56.1\ \%$

Based on this discussion, the carbon content of FeSe/C and GF@FeSe/C sample is calculated to be 16.9 % and 25.8%, respectively. To obtained the weight ratio of FeSe (w_{FeSe}), amorphous carbon (w_c) and GF (w_{GF}) in GF@FeSe/C sample, we assume that the weight ratio of FeSe to amorphous carbon in GF@FeSe/C sample is equal to the value of FeSe/C. Thus, the

values of w_{FeSe}, w_c and w_{GF} can be quantified by the following equations:

$$w_{FeSe} + w_c + w_{GF} = 1$$

$$w_c + w_{GF} = 25.8\%$$

$$w_{Fese}/w_C = (1\text{-}16.9\%)/16.9\%$$

After calculated, the amorphous carbon and GF content of GF@FeSe/C is around 15.1% and 10.7%, respectively.

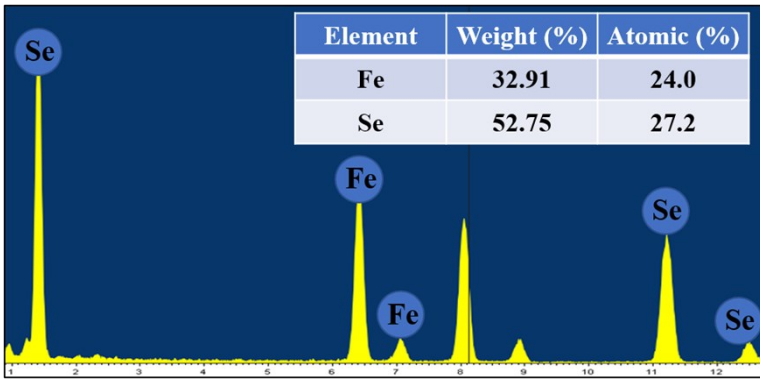

Figure S6. EDS of the GF@FeSe/C sample.

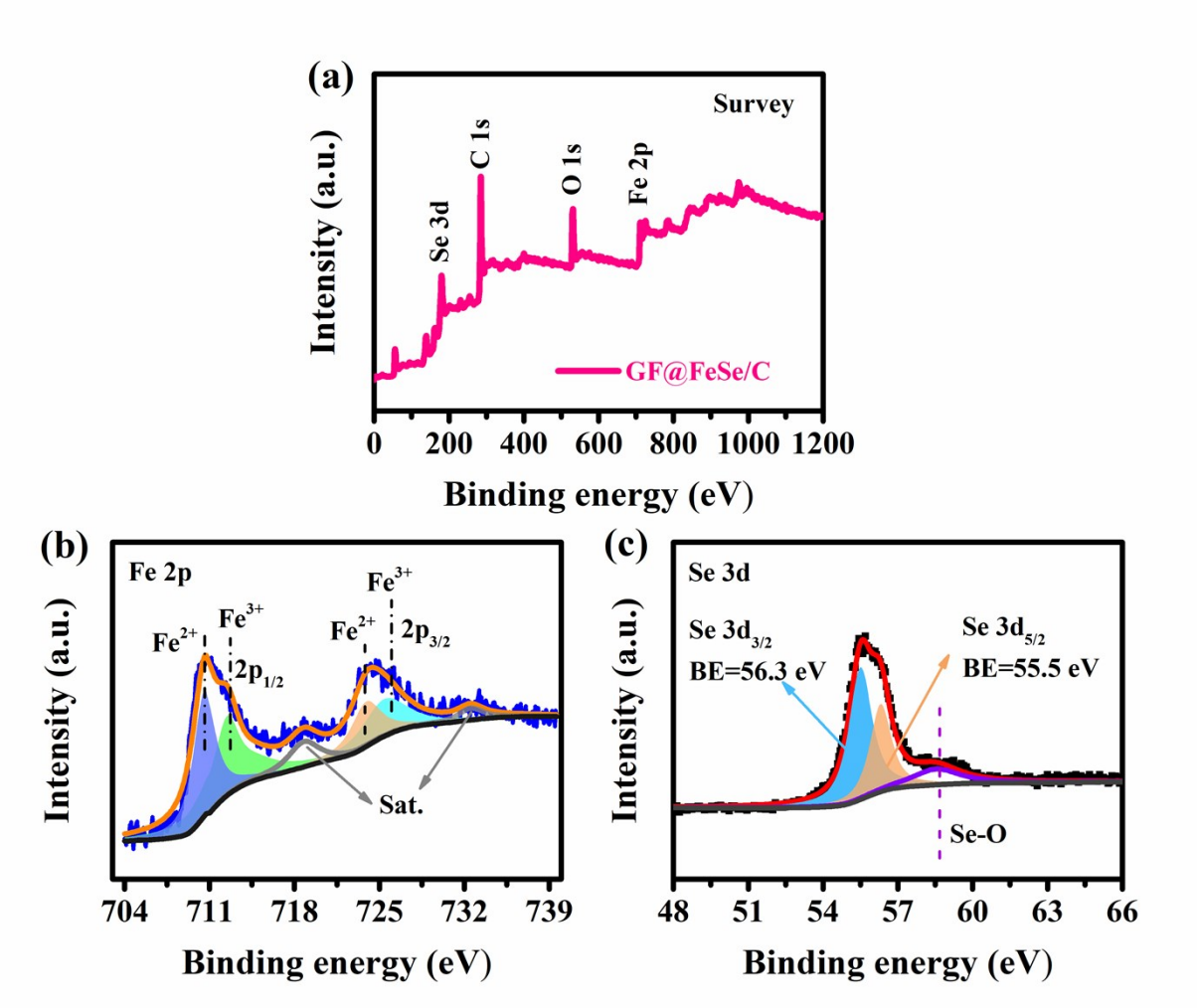

Figure S7. (a) XPS survey of GF@FeSe/C, (b) high resolution Fe 2p, and (c) Se 3d spectrum of GF@FeSe/C.

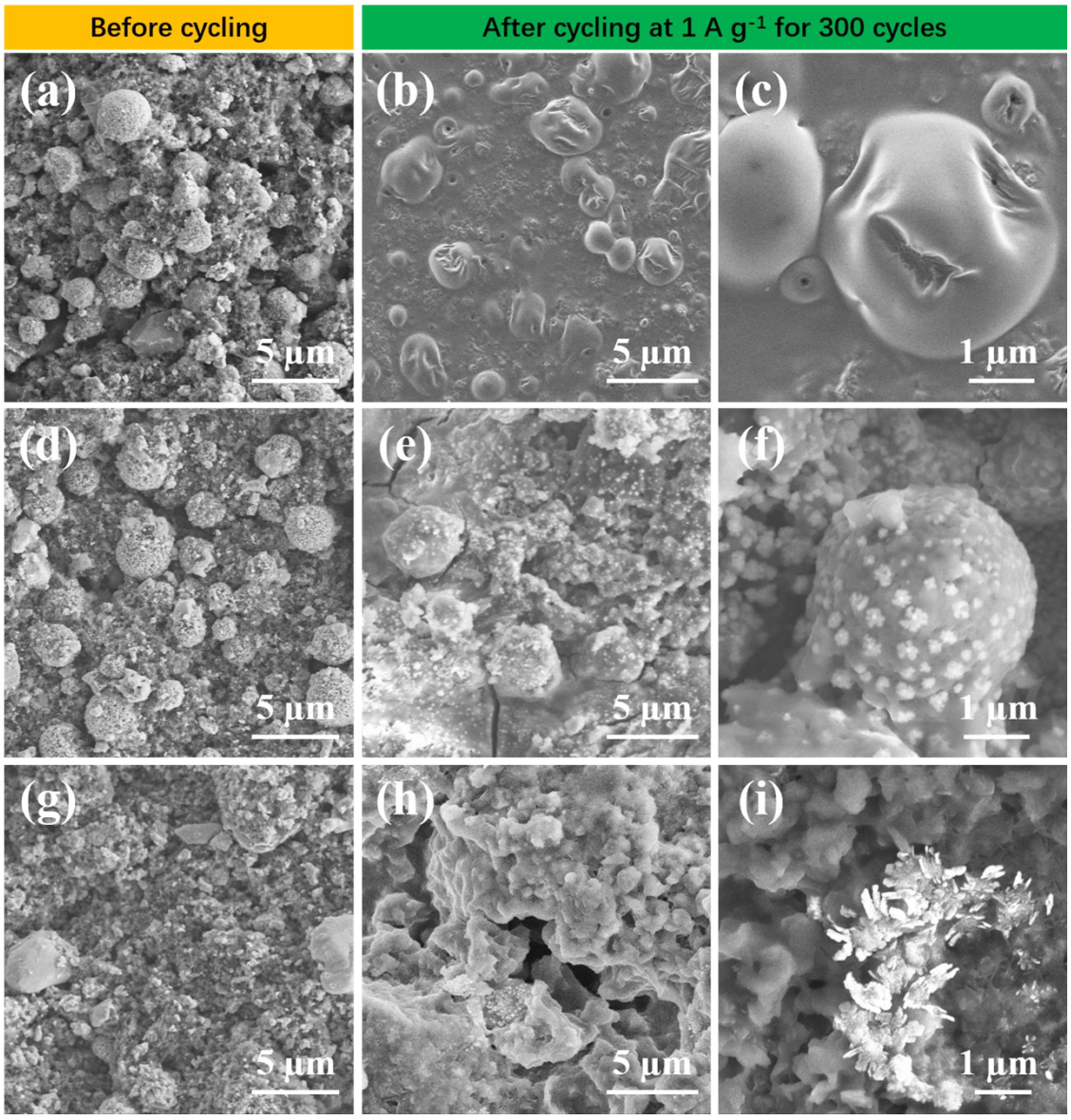

Figure S8. SEM images for (a-c) GF@FeSe/C, (d-f) FeSe/C, and (g-i) FeSe electrode before and after cycling at at 1 A g^{-1} for 300 cycles.

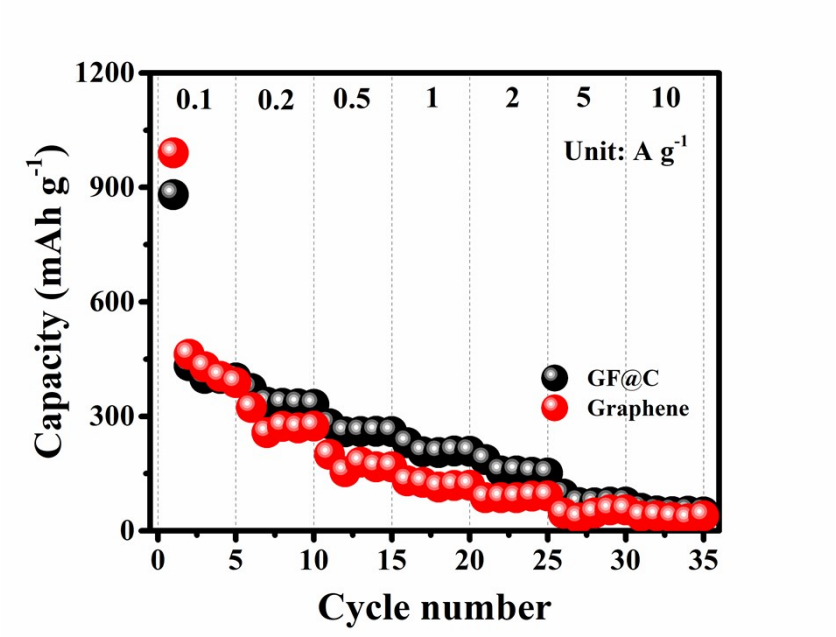

Figure S9. Rate performances of GF@C and pure graphene at different current densities in LIBs. (Note: GF@C sample is obtained by HCl etching Fe_3O_4 of GF@Fe_3O_4.)

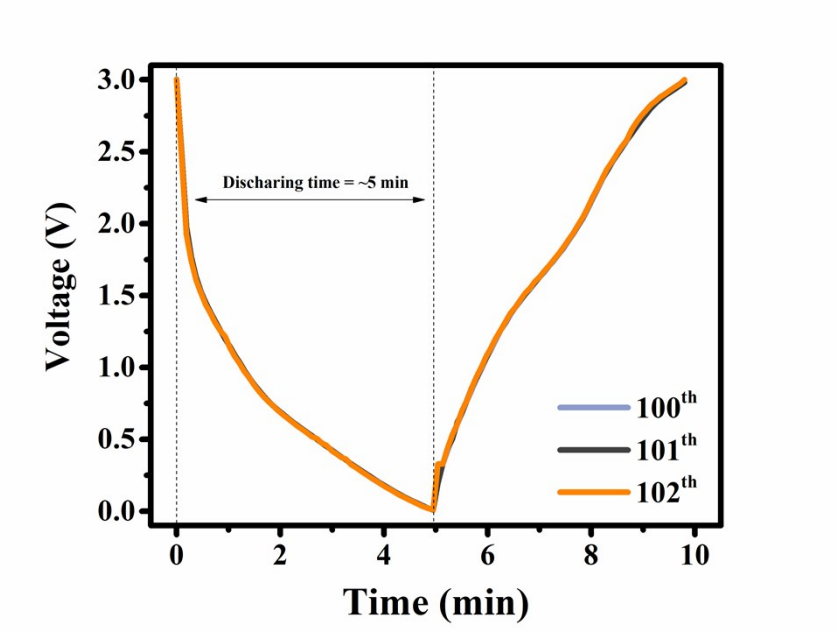

Figure S10. Voltage -time curves for GF@FeSe/C at a high current density of 5 A g^{-1}.

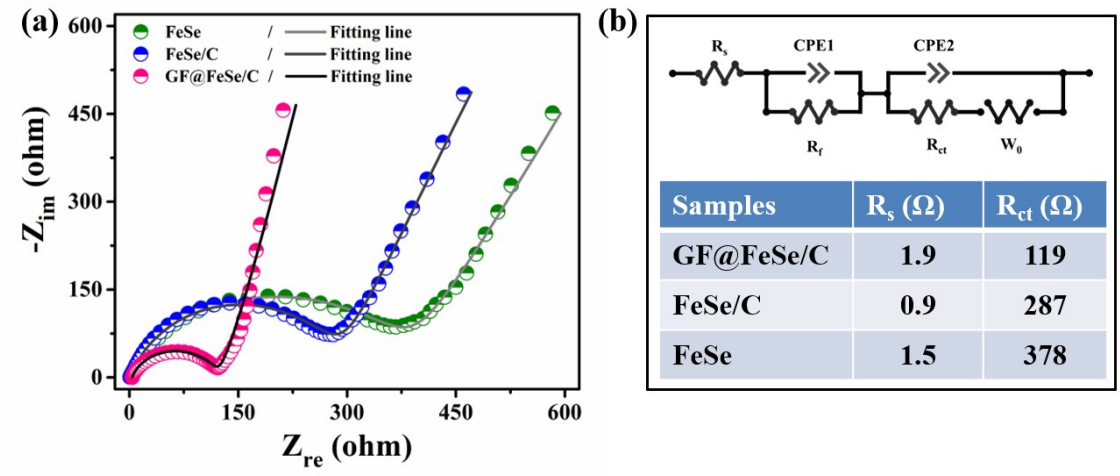

Samples	R_s (Ω)	R_{ct} (Ω)
GF@FeSe/C	1.9	119
FeSe/C	0.9	287
FeSe	1.5	378

Figure S11. (a) Nyquist plots before cycling for all as-prepared electrodes. (b) Equivalent circuit and the fitting experimental data.

Fitting details: For the equivalent electrical circuit, the intercept of the high-frequency semicircle on the Z′ axis can be attributed to the resistance of the electrolyte (Rs). The semicircle in the highand middle-frequency regions respectively represent the SEI layer resistance (R_f) and charge-transfer impedance on the electrode−electrolyte interface (R_{ct}), while the slope line at low frequency is related to the Warburg impedance (W_o) of the lithium ion diffusion. Values of Rs and Rct were also collected in inset of Figure S11b.

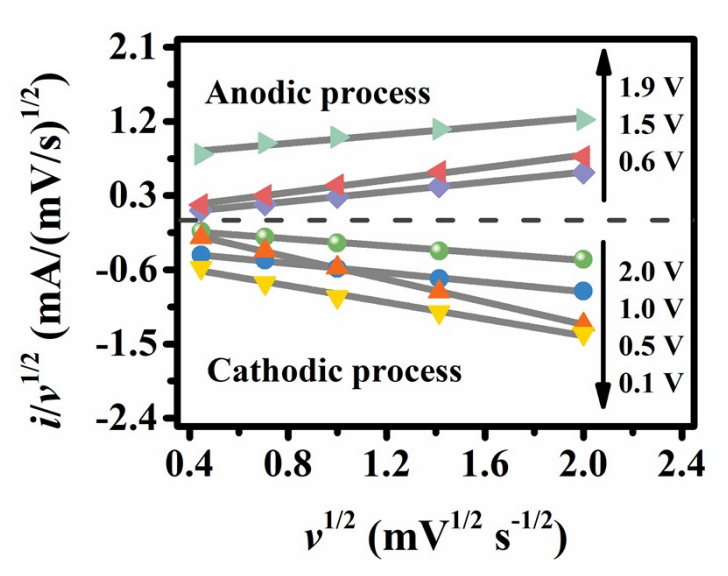

Figure S12. Liner relationship of $i/v^{1/2}$ *vs.* $v^{1/2}$ for evaluating capacitive-controlled behaviours of GF@FeSe/C.

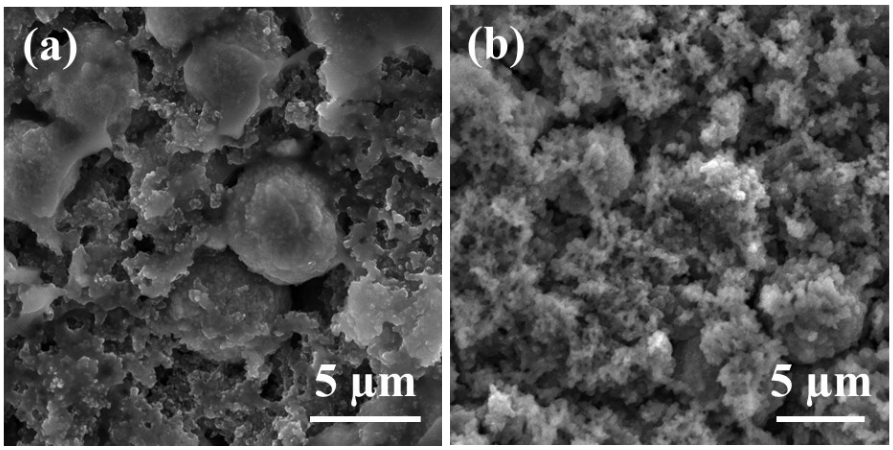

Figure S13. SEM images of GF@FeSe/C electrode cycling at 1 A g^{-1} for 100 cycles within different de-/sodiation voltage range: (a) 0.5-3.0 V and (b) 0.01-3.0 V.

As shown in **Figure S12a**, when cycling at 1 A g^{-1} within 0.5-3.0V for 100 cycles, many FeSe/C microspheres preserve their original shape, which indicate that incomplete conversion reaction will not destroy all the GF@FeSe/C integrity. However, when deep discharge to 0.01 V at 1 A g^{-1} for 100 cycles, as seen in **Figure S12b**, almost all FeSe/C microspheres are broken

into granules, indicating that a severe structure collapse caused by complete conversion reaction.

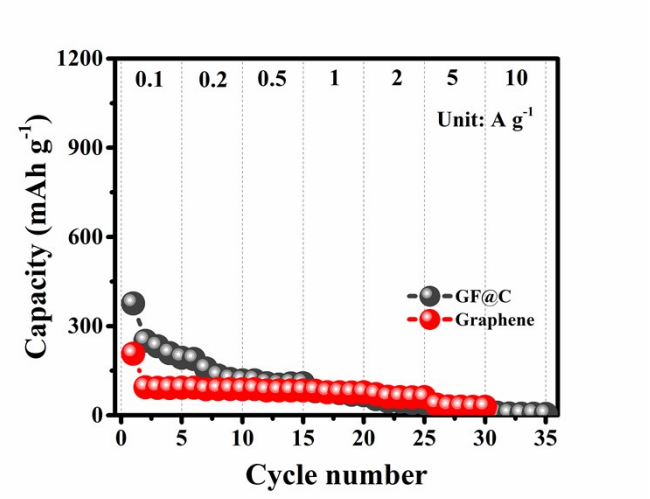

Figure S14. Rate performances of GF@C and graphene at different current densities in SIBs.

（Note: GF@C sample is obtained by HCl etching Fe_3O_4 of GF@Fe_3O_4.）

Table S1. Comparsion of the rate capability at different current densities for all three products employed in LIBs.

Rate (A g^{-1}) / Samples	0.1 2nd	0.5 7th	2.0 12nd	5.0 17th	10 22nd	15 27th	20 32nd	25 37th	30 42nd	0.1 47th
GF@FeSe/C	612	545	492	435	380	354	311	291	241	648
FeSe/C	587	404	324	281	244	221	194	173	158	420
FeSe	499	342	270	230	188	158	122	104	91	390
Note: the capacity unit is mAh g^{-1}.										

Table S2. D values based on the fitting slopes (peak1, 2, 3, 4) of Ip/$v^{1/2}$ for all samples.

D (cm^2 s^{-1}) / Samples	Peak1	Peak2	Peak3	Peak4
GF@FeSe/C	7.7×10^{-9}	4.5×10^{-8}	7.1×10^{-8}	2.0×10^{-8}
FeSe/C	—	3.1×10^{-8}	3.9×10^{-8}	—
FeSe	—	2.3×10^{-8}	3.1×10^{-8}	—

Table S3. Comparison of the lithium storage performances of previously reported selenide-based anode materials with our work.

Electrode material	Cycling stability			Rate performance		References
	Cycling number	Current density (A g^{-1})	Capability (mAh g^{-1})	Current density (A g^{-1})	Capability (mAh g^{-1})	
Hollow Structured Carbon@FeSe	200	1.6	500	1.6	620	[51]
ZnSe/CoSe@N-doped porous carbon/CNTs	1000	1	768	3	450	[52]
MOF-derived ZnSe/C@rGO	1000	2	464	5	338	[53]
CoSe/Co wrapped in carbon nanosheets	500	1	640	5	185	[54]
ZIF-67 derived CoSe@PCP	500	0.2	708	5	199	[56]
Core-shell Fe_7Se_8@C within 3D graphene	250	1	815	2	578	[57]
GF@FeSe/C	300 1200	1 5	851 332	10 30	380 241	This work

Table S4. Comparison of the sodium storage performances of previously reported selenide-based anode materials with our work.

Electrode material	Cycling stability			Rate performance		References
	Cycling number	Current density (A g^{-1})	Capability (mAh g^{-1})	Current density (A g^{-1})	Capability (mAh g^{-1})	
Ultrafine FeSe/carbon fiber	1000	2	313	5	291	[33]
FeSe/N-doped carbon	800	0.8	334	2	350	[50]
Hexagonal FeSe nanoparticles	300	0.8	230	2	272	[55]
ZIF-67 derived CoSe@PCP	100	0.1	341	4	208	[56]
$NiSe_2$/rGO composite	1000	1	346	5	318	[58]
MnSe@N-doped carbon double nanotubes	200	0.2	260	3	200	[75]
GF@FeSe/C	900	1	365	2 10	334 217	This work

References

[S1] Jing, P., Q. Wang, B. Wang, M. Xiang, H. Jiang, Y. Zhang, Y. Wei, Y. Zhang, H. Wu, and H. Liu, Facile synthesis of hierarchical polycystic iron-nitride/phosphide hybrids microsphere constructed by CNTs for stable and enhanced lithium storage. Ceram. Int., 2019, **45**, 216-224.